Laser Channeling in Millimeter-Scale Underdense Plasmas of Fast-Ignition Targets

G. Li,[1] R. Yan,[1] and C. Ren[1,2]

[1]*Department of Mechanical Engineering and Laboratory for Laser Energetics, University of Rochester, Rochester, New York 14627, USA*

[2]*Department of Physics and Astronomy, University of Rochester, Rochester, New York 14627, USA*

T.-L. Wang,[4] J. Tonge,[3] and W. B. Mori[3,4]

[3]*Department of Physics and Astronomy, University of California, Los Angeles, California 90095, USA*

[4]*Department of Electrical Engineering, University of California, Los Angeles, California 90095, USA*

(Received 27 July 2007; published 24 March 2008)

Two dimensional particle-in-cell simulations show that laser channeling in millimeter-scale underdense plasmas is a highly nonlinear and dynamic process involving longitudinal plasma buildup, laser hosing, channel bifurcation and self-correction, and electron heating to relativistic temperatures. The channeling speed is much less than the linear group velocity of the laser. The simulations find that low-intensity channeling pulses are preferred to minimize the required laser energy but with an estimated lower bound on the intensity of $I \approx 5 \times 10^{18}$ W/cm^2 if the channel is to be established within 100 ps. The channel is also shown to significantly increase the transmission of an ignition pulse.

DOI: 10.1103/PhysRevLett.100.125002 PACS numbers: 52.57.Kk, 52.38.Hb, 52.65.Rr

There are several scenarios to get an ignition pulse in fast ignition (FI) [1] close to the core of compressed fuel pellets. In the so-called "hole-boring" scenario [1], the ignition pulse needs to first propagate through a mm-scale underdense plasma to reach a critical surface with a critical density $n_c = \omega_0^2 m_e/(4\pi e^2)$ (m_e and e are electron mass and charge, respectively, and ω_0 is the pulse frequency.) There the ignition pulse may continue to push forward into the overdense plasma through its ponderomotive pressure ("hole-boring") and relativistic transparency. An alternative way to move the ignition pulse closer to the core region is to use fuel pellets with a hollow gold cone attached to one side. The first integrated FI experiments with the coned-targets showed a 10^3-times fusion neutron increase [2]. However, the hole-boring scenario is still being actively pursued for its more symmetric compression and its absence of radiation loss associated with the gold cone. Of particular concern to the hole-boring scenario is the ignition pulse energy loss through laser-plasma interactions in the mm-scale underdense plasma [3]. While a small amplitude electromagnetic wave can linearly propagate through densities less than n_c without much loss, the PW (10^{15} W) ignition pulse can interact with the plasma in a highly nonlinear manner, leading to processes such as laser self-focusing [4,5], filamentation [6,7], as well as scattering [8], and significant plasma heating and density modification [7,9]. Energy lost in this region will not be available for hole-boring and energetic electron generation at the critical surface. A channeling pulse, which could be the prepulse of the ignition pulse or a separate pulse, has been proposed [1] to produce a low-density channel to reduce the nonlinear interactions of the ignition pulse in the underdense region. Plasma density channels were created using lasers with intensities of $I = 10^{16-19}$ W/cm^2 in experiments of laser-solid target or laser-gas jet interactions [10–14]. Increased transmission of a trailing $I = 10^{20}$ W/cm^2 in the density channel was also observed [13]. Two-dimensional (2D) and three-dimensional (3D) particle-in-cell (PIC) simulations of these experiments showed laser self-focusing in the plasma and channel generation through the ponderomotive force and resulting shock expansion [12,15,16]. Most of these previous experiments and simulations were done in 100 μm-scale plasmas.

However, the underdense region of an actual FI target is about 1000 μm long. The residual plasma in the channel can continue to interact with the latter part of the channeling pulse and make the channeling process truly dynamic. In this Letter, we show for the first time that channeling in mm-scale plasmas indeed has many new phenomena that are not present in previous short-scale experiments and simulations [12,15,16], including plasma buildup to n_c in front of the laser, laser hosing or refraction, and channel bifurcation and self-correction. As a result, the channeling speed oscillates and is much less than the laser linear group velocity. These results are obtained from 2D simulations with mm-scale plasmas using the PIC code OSIRIS [17].

In our 2D PIC simulations, a channeling pulse of wavelength λ_0 is launched from the left boundary of the simulation box with a peak intensity between $I = 10^{18}$ and 10^{20} $(1\ \mu\text{m}/\lambda_0)^2$ W/cm^2 and a rise time of 150 laser periods, after which the pulse amplitude is kept constant. The transverse profile is Gaussian with a full-width-half-maximum intensity spot size of $r_0 = 16$–$47\lambda_0$ ($1/e$ spot size for the electric field, $w = 90$–$264c/\omega_0$). It is focused onto a surface $600\lambda_0$ away from the left boundary. Both s and p polarization are used to infer 3D effects. The initial plasma density profile used is $n_0 = 0.1 n_c \exp(x/L)$ with $L = 430\lambda_0$. (Length and time in these simulations are

normalized to c/ω_0 and $1/\omega_0$, respectively. But if $\lambda_0 \equiv 2\pi c/\omega_0 = 1$ μm is assumed, then the density scale length L is comparable to that of FI targets.) The ion-to-electron mass ratio is $m_i/m_e = 4590$, thereby approximating a DT plasma. The electron and ion temperatures are $T_e = T_i = 1$ keV. We simulate the region of $n_0 = 0.1$–$1.02n_c (x = 0$–$1000\lambda_0)$ in two different setups. In the first one we simulate the whole region in two separate simulations, one for $n_0 = 0.1$–$0.3n_c$ and the other for $n_0 = 0.3$–$1n_c$. The simulation box size is $L_x = 477\lambda_0$ (longitudinal) and $L_y = 262\lambda_0$ (transverse) for the low-density portion and $L_x = 523\lambda_0$ and $L_y = 262\lambda_0$ for the high density portion. The grid resolution in these simulations is $\Delta x = 0.314c/\omega_0$ and $\Delta y = 0.628c/\omega_0$. 10 particles per cell (10 PPC) are used for each species in this setup. In the second setup we simulate the entire region in one simulation with a box size of $L_x = 987\lambda_0$ and $L_y = 401\lambda_0$ (totaling 19740×4010 cells). The grid resolution is kept the same but 1 PPC is used for each species. The 10 particle/cell and the 1 particle/cell runs display qualitatively similar features in the channeling process.

We now describe general features of the channeling process using results from 10-PPC simulations where $I = 10^{19}$ W/cm^2, $r_0 = 16$ μm, and the laser was p polarized. Other simulations with different intensities and/or with an s-polarized laser display similar features. The channeling pulse power P greatly exceeds the power threshold for relativistic self-focusing P_c [5]. For $n/n_c = 0.1$, $P/P_c = 300P/(10^{12}\ \mathrm{W})n/n_c \approx 780 \gg 1$ and r_0 is $32c/\omega_p$. Therefore, relativistic whole beam self-focusing and filamentation of the pulse [4] occur before significant plasma density perturbations arise. This initial phase is dominated by filamentation that is seeded by the Gaussian transverse profile. As the laser self-focuses and filaments, the laser normalized vector potential a within each filament increases and the radius of each filaments decreases. This causes the transverse ponderomotive force from each filament to increase so that significant electron density depletion occurs [9]. The space charge force ultimately causes the ions to follow leading to the formation of several microchannels, with $n_{\max}/n_{\min} \approx 6$ [Fig. 1(a)].

Because of the fact that the microchannels form at different times along the laser propagation direction, the walls of the channels develop a longitudinal modulation. As new laser energy flows straight towards the filaments the ponderomotive force snowplows away the microchannels eventually destroying them. This leads to the formation of a single density channel centered along the axis of the laser [Fig. 1(c)]. At the end of this stage, a high-Mach-number ion acoustic shock is launched causing the walls of the channel to move radially outward at a fairly constant speed of 0.03c. The channel eventually becomes much wider than r_0. This entire process repeats as the laser and the head of the channel gradually advance toward the critical surface.

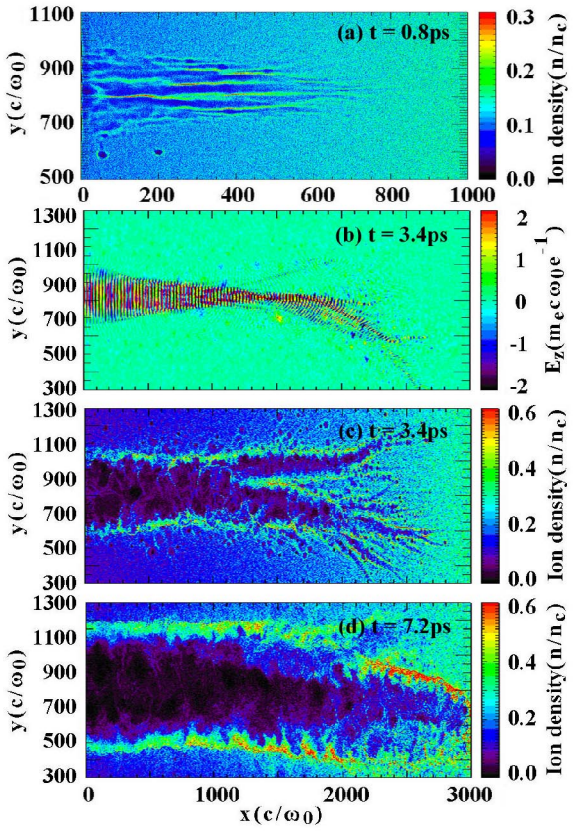

FIG. 1 (color online). Results from a simulation with an $I = 10^{19}$ W/cm^2, p-polarized laser and $n_0 = 0.1$–$0.3n_c$. (a) Ion density at $t = 0.8$ ps showing microchannels formed; (b) laser E-field showing laser hosing and (c) ion density showing channel bifurcation at $t = 3.4$ ps; (d) ion density at $t = 7.2$ ps showing channel self-correction.

While the transverse expansion is regular, the advance of the head of the channel is dynamic and intermittent. At the head of the channel the density builds up to a value significantly higher than the local value of the initial density (Fig. 2). At regions of $n_0 > 0.55n_c$, the density exceeds n_c [Fig. 2(b)], thus making the subsequent pulse propagation slower than the linear group velocity for the initial local density $v_g \equiv c\sqrt{1 - n_0/n_c}$ and more similar to hole boring. The channel can bend away from its center due to a long wavelength laser hosing instability. This is

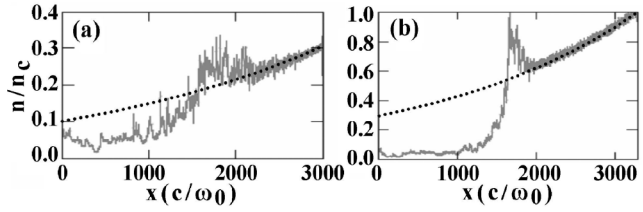

FIG. 2. Average channel density plots for (a) $n_0 = 0.1$–$0.3n_c$ at $t = 8.2$ ps and (b) $n_0 = 0.3$–$1.0n_c$ at $t = 8$ ps showing the density pileup. The dotted lines are the initial density profiles.

seeded by hosing of the head of the laser on the electron time scale as it propagates up the density gradient. For a finite-width pulse in a uniform plasma, the hosing instability [18] is caused by upward or downward tilting of local wave fronts due to a transverse phase velocity difference across the wave fronts. The phase velocity gradient is caused by the plasma density perturbation driven by the ponderomotive force of the hosing pulse [19]. The channel bends because of the hosing pulse, whose first occurrence is at $t \approx 3$ ps in the simulation with $n_0 = 0.1$–$0.3 n_c$ [Fig. 1(b)]. With the initial pulse parameters $a = 2.7$ (the normalized vector potential), $w = 90c/\omega_0$ and observed $k_h = (\pi/500)\omega_0/c$, the predicted growth rate in the long wavelength regime [19,20], $\gamma_{hu} = (a/\sqrt{8})(c/\omega_0 w)k_h c \approx 0.13\ \mathrm{ps}^{-1}$, may seem too slow for this observed time. However, self-focusing makes a larger and w smaller than their initial values and can increase γ_h. The density buildup near the laser head can also amplify the hosing through refraction.

As the channel hoses, the radius of curvature gradually increases. At some point the curvature becomes too severe to trap all of the incoming laser energy. As a consequence, some of the laser energy breaks out of the channel to form a second branch of the channel that bends in the opposite direction. This process stalls the channel formation process. Both branches then advance deeper into the plasma, leaving a narrow plasma "island" in the middle of the entire channel [Fig. 1(c)]. Eventually, the island is pushed away by the ponderomotive force of the incoming laser energy and the two branches merge to form again a single channel [Fig. 1(d)]. This process of bifurcation and self-correction can repeat in a simulation lasting ~10 ps and provides a mechanism for the head of the channel to propagate along the pulse propagation direction in our simulations.

As the plasma density in the channel center region decreases, the remaining electrons are rapidly heated to an isotropic relativistic temperature much higher than that outside the channel. At the end of the simulations, the average electron relativistic factor in the channel $\bar{\gamma} - 1 \approx 14 \gg a^2/4$ for $I = 10^{19}\ \mathrm{W/cm^2}$. The ponderomotive blowout is suppressed in plasmas with relativistic temperatures [21]. The final residual density in the channel is insensitive to the pulse intensity, $n_r \approx 0.03 n_c$.

However, the rate of the density decrease does depend on the pulse intensity. To determine T_c, the time needed for the channel to reach the critical surface, under different pulse intensities, we define the channel as any location where the average plasma density is less than $0.1 n_c$. The average density, rather than the lowest density, in the channel is more relevant for the transmission of the ignition pulse. Specifically, the density is averaged transversely around the pulse center y_c, $y_c - w/2 < y < y_c + w/2$. The channel front X_c is defined as the location when the average density decreases to $0.1 n_c$ and the channel advance speed is defined as $v_c = dX_c/dt$. In Fig. 3 we plot the time for the channel to reach different density surfaces for three pulse intensities, measured from the 1 particle-per-cell and p-polarization runs, and the resulting v_c for the $I = 10^{19}\ \mathrm{W/cm^2}$ case. It shows that v_c generally decreases as n_0 increases. However, v_c also oscillates as the channel advances, reflecting the underlying bifurcation and self-correction process seen in Figs. 1(c) and 1(d). We emphasize that v_c describes the speed of the density modification rather than the speed at which the laser energy advances. Figure 3(b) shows that v_c is much less than v_g and asymptotes to the ponderomotive hole-boring velocity [22],

$$v_{\mathrm{hb}} = 0.6c\sqrt{\frac{n_c}{n_0}\frac{m_e}{m_i}\frac{I\lambda_0^2}{10^{18}\ \mathrm{W}\,\mu\mathrm{m}^2/\mathrm{cm}^2}}, \qquad (1)$$

as the front density buildup exceeds n_c, even though the assumption of 100% laser reflection used in deriving Eq. (1) is never met in our simulation. At the end of these simulations (before the channel expansion is affected by the transverse boundary), the channel did not reach the critical surface. We estimate T_c by fitting and extrapolating the data in Fig. 3(a) and find $T_c = 283$, 72, 15 ps for $I = 10^{18}$, 10^{19}, $10^{20}\ \mathrm{W/cm^2}$, respectively. An intensity scaling can be found from this limited data set,

$$T_c \approx 2.9 \times 10^2 (I/10^{18}\ \mathrm{W/cm^2})^{-0.64}\ \mathrm{ps}, \qquad (2)$$

which enables us to obtain an intensity scaling for the total energy needed to reach the critical surface,

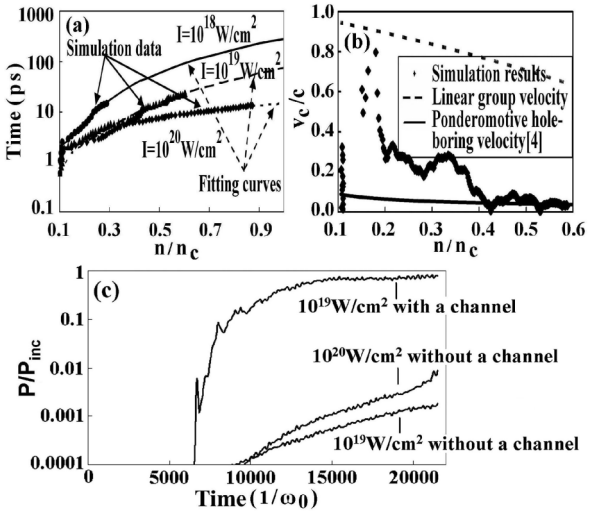

FIG. 3. (a) Time for the channel to reach different initial densities under different pulse intensities and the corresponding fitting curves. Data were taken from the 1 particle-per-cell and $n_0 = 0.1$–$1.0 n_c$ runs. (b) The channeling speed v_c in the $I = 10^{19}\ \mathrm{W/cm^2}$ case. (c) The forward Poynting flux within 1 laser spot size received at $n_0 = n_c$, normalized to that at the left entrance, for cases with and without a preformed channel.

$$E_c \approx 1.7(I/10^{18}\ \mathrm{W/cm^2})^{0.36}\,\mathrm{kJ}. \quad (3)$$

From this scaling we can see that the channeling pulse intensity should be kept as low as possible to minimize the total energy used in the channeling process. However, the ignition process needs to be completed within ~100 ps, which sets a lower bound for the channeling intensity to $I \approx 5 \times 10^{18}$ W/cm^2. If the self-focusing and other nonlinear interactions were neglected and channeling were taken to be a hole-boring process described by Eq. (1) from the beginning, analytical expressions for T_c and E_c can be obtained for density profiles dn/dx, $T_c^{(\mathrm{hb})} = \int dn(dn/dx)^{-1}/v_{\mathrm{hb}} = 2.2 \times 10^2 (I/10^{18}\ \mathrm{W/cm^2})^{-0.5} \times (L/430\ \mu\mathrm{m})\,\mathrm{ps}$ and $E_c^{(\mathrm{hb})} \approx 1.3(I/10^{18}\ \mathrm{W/cm^2})^{0.5} \times (L/430\ \mu\mathrm{m})\,\mathrm{kJ}$ for these simulations. That $T_c^{(\mathrm{hb})}$ and $E_c^{(\mathrm{hb})}$ are close to those from Eqs. (2) and (3) shows that despite the complexity of the channel formation, the channeling in these parameter regimes eventually becomes largely a ponderomotive process.

To study the effect of the channel on the transmission of the ignition pulse, we have also performed simulations with a preformed channel. The preformed channel has a plasma density of $0.05n_c$, a width the same as that of the incoming pulse ($r_0 = 16\lambda_0$), and a length of $987\lambda_0$. The plasma temperature is the same as that outside the channel (1 keV). Figure 3(c) plots the forward Poynting flux within the channel received at $n_0 = n_c$, normalized to that entering the channel front, for an $I = 10^{19}$ W/cm^2 pulse. It shows that the front end of the pulse still suffers an energy loss but the main part can have an 80% transmittance. The increased transmission is mainly due to faster heating in a lower density plasma. (An initial relativistic T_e in the channel would increase the transmittance of the front end.) In contrast, without the preformed channel, pulses of intensities of $I = 10^{19}$ and 10^{20} W/cm^2 have negligible transmission.

Compared to the p-polarization data, the s-polarization data show a slightly larger v_c but similar scalings with intensities. The difference in v_c is due to less laser absorption in the channel walls in the s-polarization case than in the p-polarization case. In reality, the difference in the laser absorption at the channel walls in the directions perpendicular and parallel to the polarization may cause different expansion rates in the two directions, resulting in a noncircular channel cross section. In addition, self-focusing is stronger in 3D than in 2D, which may lead to a larger channeling speed in 3D. These effects will be studied in future 3D simulations with reduced scales. However, phenomena such as the plasma buildup to n_c, the laser hosing/refraction, and the channel bifurcation and self-correction can only be observed in full-scale simulations, which currently can only be performed in 2D. It is worth pointing out for a typical fast-ignition target the critical surface for 1 μm light will roughly be ~600 μm in front of the target center. One way to move the channel closer to the core would be to use blue light ($\lambda = 0.35\ \mu$m) for both the channeling and ignition pulses.

This work was supported by the U.S. Department of Energy under Grants No. DE-FG02-06ER54879, No. DE-FC02-04ER54789, No. DE-FG52-06NA26195, and No. DE-FG02-03ER54721. Simulations were carried out at the National Energy Research Scientific Computing Center through an INCITE grant and on the UCLA DAWSON Cluster under Grant No. NSF-Phy-0321345. We wish to acknowledge useful discussions with Dr. R. Betti and Dr. W. Seka.

[1] M. Tabak *et al.*, Phys. Plasmas **1**, 1626 (1994).
[2] R. Kodama *et al.*, Nature (London) **412**, 798 (2001); **418**, 933 (2002).
[3] K.-C. Tzeng, W. B. Mori, and C. D. Decker, Phys. Rev. Lett. **76**, 3332 (1996).
[4] C. Max, J. Arons, and A. B. Langdon, Phys. Rev. Lett. **33**, 209 (1974).
[5] G.-Z. Sun, E. Ott, Y. C. Lee, and P. Guzdar, Phys. Fluids **30**, 526 (1987).
[6] P. Kaw, G. Schmidt, and T. Wilcox, Phys. Fluids **16**, 1522 (1973).
[7] A. B. Langdon and B. F. Lasinski, Phys. Rev. Lett. **34**, 934 (1975).
[8] D. W. Forslund, J. M. Kindel, and E. L. Lindman, Phys. Fluids **18**, 1002 (1975).
[9] W. B. Mori *et al.*, Phys. Rev. Lett. **60**, 1298 (1988).
[10] P. E. Young *et al.*, Phys. Rev. Lett. **75**, 1082 (1995); Phys. Plasmas **2**, 2825 (1995).
[11] M. Borghesi *et al.*, Phys. Rev. Lett. **78**, 879 (1997).
[12] J. Fuchs *et al.*, Phys. Rev. Lett. **80**, 1658 (1998).
[13] A. J. Mackinnon *et al.*, Phys. Plasmas **6**, 2185 (1999).
[14] K. A. Tanaka, H. Hashimoto, R. Kodama, K. Mima, Y. Sentoku, and K. Takahashi, Phys. Rev. E **60**, 3283 (1999).
[15] A. Pukhov and J. Meyer-ter-Vehn, Phys. Rev. Lett. **76**, 3975 (1996).
[16] Y. Sentoku, W. Kruer, M. Matsoka, and A. Pukhov, Fusion Sci. Technol. **49**, 278 (2006).
[17] R. G. Hemker, Ph.D. thesis, UCLA, 2000; R. A. Fonseca *et al.*, *Lecture Notes in Computer Science* (Springer-Verlag, Heidelberg, 2002), Vol. 2331, p. 342.
[18] G. Shvets and J. S. Wurtele, Phys. Rev. Lett. **73**, 3540 (1994); P. Sprangle, J. Krall, and E. Esarey, Phys. Rev. Lett. **73**, 3544 (1994).
[19] C. Ren and W. B. Mori, Phys. Plasmas **8**, 3118 (2001).
[20] B. J. Duda and W. B. Mori, Phys. Rev. E **61**, 1925 (2000); B. J. Duda *et al.*, Phys. Rev. Lett. **83**, 1978 (1999).
[21] K.-C. Tzeng and W. B. Mori, Phys. Rev. Lett. **81**, 104 (1998).
[22] S. C. Wilks, W. L. Kruer, M. Tabak, and A. B. Langdon, Phys. Rev. Lett. **69**, 1383 (1992).